nature portfolio

https://doi.org/10.1038/s41592-021-01081-y

## Supplementary information

# Single-molecule FRET imaging of GPCR dimers in living cells

In the format provided by the authors and unedited

# SUPPLEMENTARY INFORMATION

## Single-Molecule FRET Imaging of GPCR Dimers in Living Cells

Wesley B. Asher[1,2,3], Peter Geggier[1,3], Michael D. Holsey[4], Grant T. Gilmore[5], Avik K. Pati[7], Jozsef Meszaros[1,3], Daniel S. Terry[7], Signe Mathiasen[1,3], Megan J. Kaliszewski[5], Mitchell D. McCauley[5], Alekhya Govindaraju[3], Zhou Zhou[6,11], Kaleeckal G. Harikumar[8], Khuloud Jaqaman[9,10], Laurence J. Miller[8], Adam W. Smith[5], Scott C. Blanchard[6,7,*], Jonathan A. Javitch[1,2,3,4,*]

1. Department of Psychiatry, Vagelos College of Physicians and Surgeons, Columbia University, New York, NY, USA
2. Department of Molecular Pharmacology and Therapeutics, Vagelos College of Physicians and Surgeons, Columbia University, New York, NY, USA
3. Division of Molecular Therapeutics, New York State Psychiatric Institute, New York, NY, USA
4. Department of Physiology and Cellular Biophysics, Vagelos College of Physicians and Surgeons, Columbia University, New York, NY, USA
5. Department of Chemistry, University of Akron, Akron, OH, USA
6. Department of Physiology and Biophysics, Weill Cornell Medicine, New York, NY, USA
7. Department of Structural Biology, St. Jude Children's Research Hospital, Memphis, TN, USA
8. Department of Molecular Pharmacology and Experimental Therapeutics, Mayo Clinic, Scottsdale, AZ, USA
9. Department of Biophysics, University of Texas Southwestern Medical Center, Dallas, TX, USA
10. Lyda Hill Department of Bioinformatics, University of Texas Southwestern Medical Center, Dallas, TX, USA
11. Present address: Department of Chemistry, Queensborough Community College, The City University of New York, Bayside, NY, USA

*Correspondence should be addressed to:
J.A.J.: Jonathan.Javitch@nyspi.columbia.edu and S.C.B.: Scott.Blanchard@STJUDE.ORG

**CONTENTS**

## SUPPLEMENTARY FIGURES

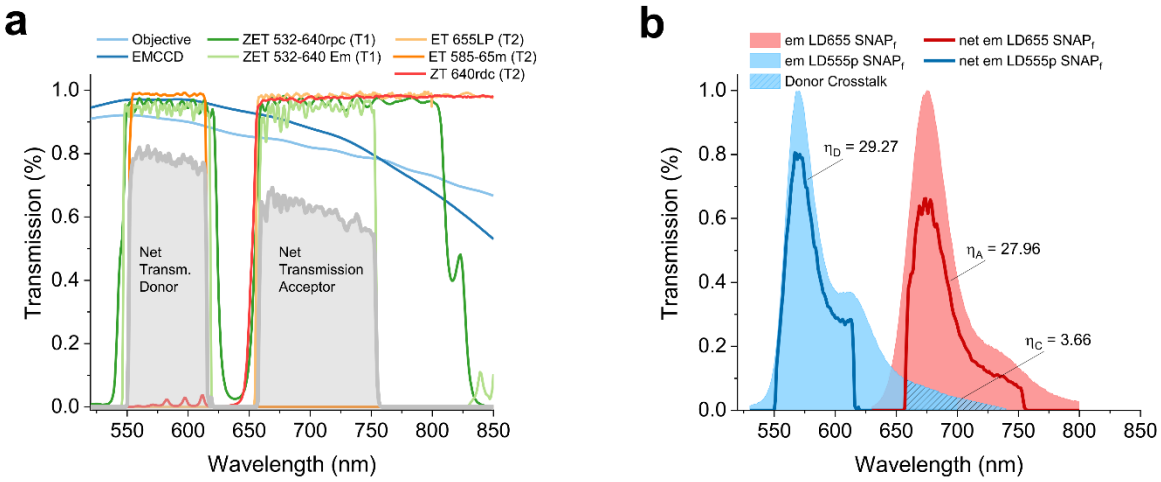


**Supplementary Figure 1**. Calculation of the net emission spectrum and determination of the gamma ($\gamma$) and crosstalk correction factors. (**a**) Spectral transmission profiles of the objective (100x, NA 1.7), the electron multiplying CCD sensor, and the main optical filters in the upper (T1) and lower (T2) light path of the microscope as discussed in **Methods**. The estimated net transmission of all elements is shown in gray. (**b**) Normalized emission spectra of the LD555p-SNAP$_f$ (donor, blue) and LD655-SNAP$_f$ (acceptor, red). The net emission spectra (*net em*) were calculated from the product of the net-optical transmission and the normalized dye emission spectra. Additionally, the detection efficiencies $\eta_D$ (donor emission channel) and $\eta_A$ (acceptor emission channel) can be calculated by integration over the net emission spectra. Using the ratio of the detection efficiencies $\eta_A/\eta_D$ and the ratio of the fluorescence quantum yields $\Phi_{A/D} = \Phi_A/\Phi_D$ (**Supplementary Table 1,** $\Phi_{A/D} = 1.26$) the correction factor $\gamma = \eta_{A/D} \cdot \Phi_{A/D}$ can be calculated as 1.20. The integrated donor emission that bleeds into the acceptor channel $\eta_C$ is a measure of the spectral donor crosstalk. An estimate of the crosstalk correction factor can be calculated from the detection efficiency ratio $\eta_C/\eta_D$ (ratio of the donor signal in the acceptor emission channel to the donor signal in the donor emission channel.) and is approximately 0.13.

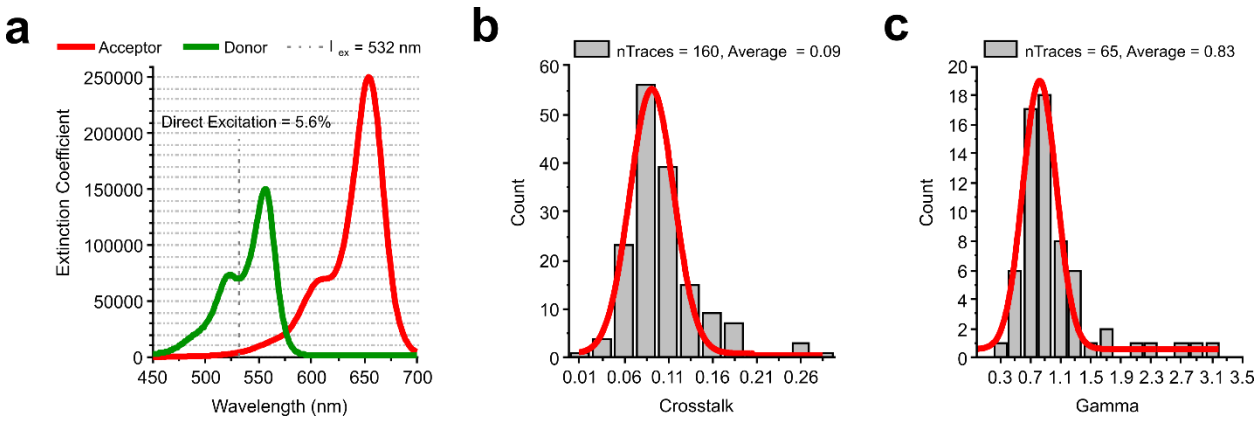


**Supplementary Figure 2**. Determination of correction factors for direct excitation, crosstalk and fluorescence detection. **(a)** Extinction spectra of the LD FRET dye pair with the donor excitation line at 532 nm. The fraction of direct excitation at 532 nm was estimated from the spectra to be 5.6%. **(b)** Histogram of individual crosstalk values measured from anticorrelated donor and acceptor fluorescence traces in live and fixed cells. F. The mean crosstalk value of 0.09 was determined by Gaussian fitting. **(c)** Histogram of individual gamma values measured from anticorrelated donor and acceptor fluorescence traces in live cells. For the determination of the gamma value we analyzed only traces of mGluR2 receptors, where the receptors were either in immobile or free diffusion mode. The mean gamma of 0.83 was determined by Gaussian fitting. These experimentally determined values for crosstalk and gamma differ somewhat from the theoretically determined values shown in Supplementary Figure 11, likely due to differences in the experimental environments and the additional optical components present in the single-molecule experiments.

## SUPPLEMENTARY TABLES

**Supplementary Table 1.** Photophysical data for recombinantly expressed and purified $SNAP_f$ labeled with LD555p or LD655. $\lambda_{abs}$, $\lambda_{em}$, $\Phi_F$, $\tau_F$, and $r_{ss}$ are the absorption maximum wavelength, emission maximum wavelength, fluorescence quantum yield, fluorescence lifetime, and steady-state fluorescence anisotropy, respectively.

| Fluorophore-$SNAP_f$ | $\lambda_{abs}$ (nm) | $\lambda_{em}$ (nm) | $\Phi_F$ | $\tau_F$ (ns) | $r_{ss}$ |
|---|---|---|---|---|---|
| LD555p | 558 | 570 | 0.47 ± 0.02 | 1.90 ± 0.02 | 0.30 ± 0.01 |
| LD655 | 657 | 675 | 0.59 ± 0.02 | 2.09 ± 0.02 | 0.30 ± 0.01 |

**Supplementary Table 2.** Photophysical properties of smFRET within $S_f$-mGluR2 labeled with LD555p (donor) and LD655 (acceptor) in CHO cells under select conditions. Cells were imaged as described at a frame rate of 25 Hz and were either fixed with PFA where molecules are immobilized (Fixed) or imaged under live cell conditions and trajectories were selected by FDT analysis (Live). The mean intensity, lifetime, and calculated photon budget are shown. The lifetime values were determined by single-exponential fits from cumulative distributions (Methods). Acceptor intensity and total intensity values are during FRET with 532 nm excitation. Donor intensity values were calculated from donor intensity distributions generated from data measured in the absence of FRET.
*Because the duration of smFRET trajectories during diffusion in living cells is limited not by acceptor or donor fluorophore photobleaching but rather by issues related to tracking single molecules, we do not report photon budgets for live cell measurements.

| Condition | Dye | Mean Intensity (photons/frame) | Lifetime (s) | Photon Budget (photons) |
|---|---|---|---|---|
| Fixed | Donor | 470 | 51 | 598,075 |
| Fixed | Acceptor - FRET | 279 | 19 | 132,525 |
| Fixed | Total - FRET | 458 | — | — |
| Live | Donor | 504 | 2.5 | * |
| Live | Acceptor - FRET | 190 | 2.4 | * |
| Live | Total - FRET | 457 | — | — |

**Supplementary Table 3.** Optimized u-track parameters used for donor- and acceptor-particle tracking.

| **Input parameters** | **Donor** | **Acceptor** |
|---|---|---|
| *Spot detection parameters* | | |
| Psf-sigma | 0.85 pixels | 0.85 pixels |
| Mixture-model fitting | 1 | 1 |
| Alpha value for initial detection of local maxima | 0.01 | 0.01 |
| Integration window | 1 | 1 |
| **testAlpha R, A, D, F** | 0.05, 0.05, 0.05, 0 | 0.05, 0.05, 0.05, 0 |
| *General tracking parameters* | | |
| Time window | 5 frames | 5 frames |
| **Flag for merging and splitting** | 0 | 0 |
| Minimum track segment length | 2 fames | 2 frames |
| *Frame-to-frame linking parameters* | | |
| Flag for linear motion | 0 | 0 |
| Search radius lower limit | 1.5 pixels | 2 pixels |
| Search radius upper limit | 3 pixels | 3 pixels |
| Std dev multiplication factor | 4 | 4 |
| Flag for using local density | 1 | 1 |
| Number of frames used in nearest neighbor calculation | 5 | 5 |
| *Gap closing, merging and splitting parameters* | | |
| Flag for linear motion | 0 | 0 |
| Search radius lower limit | 2.5 pixels | 3 pixels |
| Search radius upper limit | 3 pixels | 3 pixels |
| Std dev multiplication factor | [4 4 4 4 4] | [4 4 4 4 4] |
| Brownian scaling | [0.25, 0.25] | [0.25, 0.25] |
| timeReachConfB | 5 | 5 |
| Amplitude ratio lower and upper limit | [0.7, 4] | [0.7, 4] |
| Min length for track segment analysis | 5 | 5 |
| Flag for using local density | 0 | 0 |
| Number of frames used in nearest neighbor calculation | 5 | 5 |
| linStdMult | [1 1 1 1 1] | [1 1 1 1 1] |
| linScaling | [0.25 0.01] | [0.25 0.01] |
| timeReachConfL | 5 | 5 |
| Max angle between the directions of motion | 45 | 45 |
| Gap penalty | 1.5 | 1.5 |
| gapExcludeMS | 1 | 1 |
| strategyBD | -1 | -1 |

**Supplementary Table 4.** Comparison of different experimental conditions for detection and tracking of smFRET. CHO cells stably expressing $S_f$-mGluR2 (conditions 1,2,4,5) or Halo-mGluR2 (condition 3) were labeled with the indicated fluorophores and imaged as described in the Methods with the indicated NA TIRF objective under the temperature and oxygen conditions described. Identical donor laser power was used for imaging all conditions. Data were analyzed in the pipeline to obtain freely diffusing traces and the mean smFRET acceptor intensity from a Gaussian fit of the data is shown. The smFRET durations were determined by an exponential fit of cumulative data. Data from each condition were determined from 10-16 cells.

| Condition | Self-labeling tag | Fluorophore Pair | Objective NA | Temperature/ oxygen conditions | Mean acceptor intensity | Duration of smFRET (s) |
|---|---|---|---|---|---|---|
| 1 | $SNAP_f$ | LD555p-LD655 | 1.70 | 23 °C /50% reduced | $204 \pm 10$ | $2.55 \pm 0.06$ |
| 2 | $SNAP_f$ | DY549P1-AF647 | 1.70 | 23 °C /50% reduced | $165 \pm 8$ | $2.02 \pm 0.02$ |
| 3 | HaloTag | LD555p-LD655 | 1.70 | 23 °C /50% reduced | $114 \pm 0.2$ | $1.55 \pm 0.02$ |
| 4 | $SNAP_f$ | LD555p-LD655 | 1.49 | 23 °C /50% reduced | $140 \pm 17$ | $2.03 \pm 0.03$ |
| 5 | $SNAP_f$ | LD555p-LD655 | 1.70 | 37 °C /ambient | $203 \pm 10$ | $1.40 \pm 0.01$ |

**Supplementary Table 5:** Criteria for NLT analysis.

| Type | Criteria | Notes |
|---|---|---|
| Signal-Bgd Ratio: s | $s_{min} = 1.4$<br>$s_{max} = 2.2$ | All traces t that have a mean signal to background ratio in the interval $S = \{ s \mid 1.4 < s < 2.2 \}$ are selected. |
| Crosstalk Value: crt | $crt_{min} = 0.3$<br>$crt_{max} = 10$ | All traces t that have a crosstalk value in the interval $Crt = \{ crt \mid 0.3 < crt < 10 \}$ are selected. |
| Total Intensity: int | $int_{min} = 450$ | All traces t that have a mean total intensity value in the interval $Int = \{ int \mid int > 450 \}$ are selected. |
| Multiple Events: logical<br><br>$d_c$: the centroid distance between reoccurring track segments<br>n: the number of reoccurring track segments<br>t: the length of track segments in frames | $d_c = 1.5$ pixels<br>n = 25 events<br>$t_{limit} = 0.5$s | If a trajectory $\theta_i$ that belongs to a series of trajectories $X = \{\theta_k^X, k = 1 \dots n \mid n > 25\}$ re-appears at the same location (centroid distance $d(\theta_i \mid X) < 1.5\ pixels$) AND the mean track lifetime of X < $t_{limit}$ then the analysis returns:<br>logical 0 ( $\theta_i$ is rejected)<br>else<br>logical 1 ( $\theta_i$ is selected) |

A single molecule trace t is accepted if $t \in S\ AND\ t \in Crt\ AND\ t \in Int$. Re-appearing trajectories are removed by the multiple events criteria as described above.

**Supplementary Table 6.** Summary of experimental parameters obtained from the PIE-FCCS measurements. Unless otherwise noted, the values are reported as the mean ± standard error. $\langle N_R \rangle$, $\langle N_G \rangle$, and $\langle N_{RG} \rangle$ represent average population of red, green and co-diffusing species respectively. The fraction correlated ($f_c$) values are reported as both mean and median measurements. Molecular brightness values for red and green labels, $\eta_R$ and $\eta_G$, are reported in photon counts per second per molecule (cpsm) for each protein. The diffusion coefficients ($D_{R/G}$) are calculated from the $\tau_D$ values, and receptor density values are determined from the amount of labeled receptors for red, green or both within the confocal volume.

| **Parameter** | **Sample** | | | | |
|---|---|---|---|---|---|
| | **$S_f$-TM-LDL** | **$S_f$-mGluR2** | **$S_f$-Δ2Δ** | **$S_f$-MOR** | **$S_f$-SecR** |
| Number of Cells | 28 | 89 | 70 | 84 | 63 |
| $\langle N_R \rangle$ | 17 ± 2 | 16 ± 1 | 15 ± 2 | 11 ± 1 | 18 ± 1 |
| $\langle N_G \rangle$ | 24 ± 3 | 16 ± 1 | 14 ± 1 | 9 ± 0 | 16 ± 1 |
| $\langle N_{RG} \rangle$ | 15615 ± 4834 | 106 ± 7 | 12243 ± 2536 | 27094 ± 3849 | 798 ± 554 |
| $f_c$ (mean) | 0.037 ± 0.007 | 0.181 ± 0.005 | 0.032 ± 0.004 | 0.036 ± 0.005 | 0.107 ± 0.006 |
| $f_c$ (median) | 0.035 | 0.184 | 0.027 | 0.021 | 0.106 |
| $D_R$ ($\mu m^2 \cdot s^{-1}$) | 0.334 ± 0.025 | 0.265 ± 0.011 | 0.244 ± 0.010 | 0.300 ± 0.011 | 0.222 ± 0.011 |
| $D_G$ ($\mu m^2 \cdot s^{-1}$) | 0.489 ± 0.033 | 0.257 ± 0.011 | 0.281 ± 0.014 | 0.334 ± 0.012 | 0.224 ± 0.011 |
| $\eta_R$ (cpsm) | 1250 ± 44 | 1073 ± 66 | 628 ± 37 | 459 ± 17 | 464 ± 19 |
| $\eta_G$ (cpsm) | 851 ± 54 | 743 ± 42 | 524 ± 25 | 308 ± 16 | 301 ± 13 |
| $\tau_{D,CCF}$ (ms) | - | 75 ± 9 | - | - | 450 ± 69 |
| Density (Red) (molecules/$\mu m^2$) | 100 ± 11 | 99 ± 7 | 90 ± 11 | 64 ± 4 | 109 ± 8 |
| Density (Green) (molecules/$\mu m^2$) | 173 ± 22 | 113 ± 7 | 99 ± 10 | 62 ± 3 | 115 ± 8 |
| Total Density (molecules/$\mu m^2$) | 266 ± 32 | 210 ± 13 | 188 ± 20 | 126 ± 7 | 223 ± 15 |

**Supplementary Table 7.** Correction factors used for smFRET calculations. The spectral crosstalk and detection correction were measured experimentally and are shown in **Supplementary Figure 2**. The direct excitation was estimated based on the spectral properties of the LD dyes and the filters used.

| Correction | | Global correction factors |
|---|---|---|
| Spectral crosstalk | $\alpha$ | 0.09 |
| Direct excitation | $\delta$ | 0.056 |
| Detection correction | $\gamma$ | 0.83 |

## SUPPLEMENTARY NOTE 1

### Limitations of tracking cell-surface receptors imaged by TIRF

The loss of tracking of a single TM-protein complex within the plasma membrane before fluorophore photobleaching can result from a variety of processes. Because the TIRF-excitation field decays exponentially over ~100 nm above the coverslip[1], only those fluorescently-labeled receptors that diffuse in the plasma membrane (~10 nm) nearest in proximity to the coverslip are excited. Therefore, labeled receptors outside the TIRF field, which include those in the apical-plasma membrane or within endosomes and other organelles, are not excited (or only very weakly and evade detection). Particle detection and tracking will be lost for receptors that diffuse laterally out of the TIRF field during measurement, which can occur for receptors near the cell edge that diffuse into the apical membrane, but also for those that move in the z plane by diffusing into plasma membrane regions that are further in proximity from the glass substrate due to variation in cell morphology and adhesion[2-4]. Receptors may also internalize by endocytosis and exit the field[1]. In addition, known local variances in refractive index associated with TIRF imaging of adherent cells can produce field inhomogeneities that could cause fluctuations in fluorescence intensities of diffusing particles[2]. Therefore, if a particle diffuses within a region of the field with reduced excitation power and its intensity drops below the detection threshold for longer than the gap-closing time window, tracking will end.

Notably, to retain the identity of each smFRET trajectory, merging-and-splitting of particles was not used during tracking (**Supplementary Table 3**)[5], since the identity of each particle is lost when they merge, and lifetimes can no longer be calculated even if they split. Therefore, if the acceptor signals of two or more particles exhibiting smFRET merge, tracking for both particles end to avoid signal colocalization. This clearly leads to artificial truncation of many trajectories but cannot be avoided without going to even lower-receptor densities where receptor interactions are even less likely to occur.

## SUPPLEMENTARY NOTE 2

### Comparison of different experimental conditions for detection and tracking of smFRET

We also explored whether other experimental conditions could be used for detection and tracking of smFRET within mGluR2 dimers to demonstrate broader applicability as well as to support our choices regarding the optimal components of our methodology. These included the use of the commercially available cyanine-based fluorophores DY549P1 and AF647 for $SNAP_f$ labeling that we have explored previously[6,7], as well as the use of self-labeling HaloTag instead of $SNAP_f$, labeled with chloroalkane-conjugated LD555p and LD655 (**Methods**). Of the available self-labeling tags, SNAP tags have been used most frequently in GPCR studies and are the only such tag that has been used for smFRET of purified reconstituted proteins, and thus seemed the best choice for developing smFRET to study GPCR interactions in living cells[8,9]. $SNAP_f$ is an improved version of the first generation SNAP tag with faster labeling kinetics[10,11], which is desirable for cell-based studies, particularly for FRET where efficient labeling is essential.

We also used a 1.49 NA TIRF objective or imaged at 37 °C and ambient oxygen, instead of using a 1.70 NA TIRF objective and imaging at 23 °C and partial oxygen depletion, the conditions used for all our other single-molecule experiments (**Methods**).

While smFRET was observed for each condition, the most robust signals, assessed by the mean acceptor intensity and duration of tracked smFRET, was observed with $SNAP_f$ labeled with LD555p and LD655, imaged using the higher NA objective in a partially reduced oxygen environment at room temperature (**Supplementary Table 4; Methods**). Thus, we employed these optimal combinations of conditions for investigations of receptor conformational dynamics and dimerization.

## SUPPLEMENTARY NOTE 3

### FRET efficiency histogram comprised of immobile/confined segments for $S_f$-mGluR2

To address whether the receptor configuration in the immobile/confined substates differs from that of freely diffusing receptors, we generated the FRET-efficiency histogram for $S_f$-mGluR2 comprised only of the immobile/confined segments of single-molecule traces that also include segments of free diffusion. The FRET histograms were similar to that of the freely diffusing segments, with the notable exception that immobile and confined substates exhibited a small additional lower-FRET value component (**Extended Data Fig. 4i**). This lower-FRET state may reflect a distinct receptor conformation in immobile and confined microdomains or a state also present in diffusing receptors that is more readily detected in immobile and confined substates.

## SUPPLEMENTARY NOTE 4

### Non-limited lifetime trajectory (NLT) selection analysis

The requirement that a trajectory last at least 20 frames provided assurance that only bona fide molecules with sufficiently bright and stable fluorescence traces were selected, such that only a total intensity-based filter was required for selecting trajectories by FDT analysis. In contrast, when we included trajectories as short as 2 frames, many spurious trajectories were collected. We removed these trajectories using NLT analysis to ensure that only bona fide smFRET trajectories representing fluorophore-labeled receptors were selected.

## SUPPLEMENTARY NOTE 5

### Purification and labeling of recombinantly expressed $SNAP_f$

The $SNAP_f$-$CLIP_f$ protein was expressed from the pET51b–$SNAP_f$–$CLIP_f$ vector (gift from Kai Johnsson, Max Plank Institute for Medical Research) in *E. coli* and purified by Ni-NTA chromatography followed by Strep-Tactin superflow as previously described[12]. The $SNAP_f$ domain of the purified protein was labeled with LD555p-BG and LD655-BG by adding 1.2-fold excess of each dye to the protein in phosphate-buffered saline pH 7.4 (PBS) in presence of 1 mM 1,4-dithiothreitol (DTT) at room temperature. The reaction was incubated in the dark for 1 hr. Unreacted dye was removed using Strep-Tactin superflow. The labeled protein was purified using a Superdex 75 HiLoad 16/60 gel filtration column (GE Healthcare) in phosphate-buffered saline (pH 7.4) and 1 mM DTT.

## SUPPLEMENTARY NOTE 6

### Plasmid construction and BRET-Based cAMP assays

Plasmids coding for amino-terminal $SNAP_f$-tagged TM proteins were constructed using standard sub-cloning methods by replacing the dopamine D2 receptor coding region of the previously described pcDNA5/FRT/TO-IRES SNAPfast-D2 vector[13] with the following coding regions: human mGluR2 (positions 20-872); TM-LDL (positions 786-820 of the human LDL receptor); Δ2Δ, positions 557-857 of human mGluR2); human MOR); and human SecR (positions 22-440). The amino-terminal Halo-tagged mGluR2 vector was constructed by replacing the $SNAP_f$ coding region of the $SNAP_f$-mGluR2 vector described above with the HaloTag (Promega) coding region. In these vectors, the Kozac sequence was mutated to thymines at the -3 and +4 positions to produce a weak Kozac sequence, and the CMV enhancer sequence was partly deleted by digestion of the vector with NruI and SnaBI and subsequent

religation to generate a crippled CMV promoter (**Extended Data Fig. 1c**). All constructs were confirmed by DNA sequencing (Macrogen).

Bioluminescence resonance energy transfer (BRET)-based cAMP inhibition or generation assays were carried out in CHO FlpIn (Invitrogen) cells transiently transfected using lipofectamine LTX (Invitrogen) per manufacturer's protocol. For the mGluR2 and MOR-mediated cAMP inhibition assay, the pcDNA5/FRT/TO-IRES vectors encoding either $S_f$-mGluR2 (0.5 μg) or $S_f$-MOR (0.1 μg) and plasmids encoding the cAMP sensor using YFP-Epac-RLuc (CAMYEL[14], 1 μg, ATCC), $G\alpha_{i1}$ (0.167 μg), $G\beta_1$ (0.5 μg), and $G\gamma_2$ (0.5 μg) were transfected. For the SecR-mediated cAMP generation assay, the pcDNA5/FRT/TO-IRES vector encoding $S_f$-SecR (0.5 μg) and plasmids encoding CAMYEL (1 μg), $G\alpha_s$ (0.167 μg), $G\beta_1$ (0.5 μg), and $G\gamma_2$ (0.5 μg) were transfected. Cells were prepared and assayed as described previously in detail using a 96-well microplate and Pherastar FS plate reader[15]. After incubation with coelentrazine H (5 μM, Dalton Pharma Services) for 8 minutes, DCG-IV (Tocris Biosceince), [D-Ala$^2$, N-MePhe$^4$, Gly-ol]-enkephalin (DAMGO) (MilliporeSigma), or human secretin peptide (MilliporeSigma) was injected for assays involving $S_f$-mGluR2, $S_f$-MOR, and $S_f$-SecR, respectively. For cAMP inhibition assays, 30 μM forskolin (Cayman Chemical Company) was added to the cells 10 minutes prior to injection of receptor ligand. BRET measurements were taken 30 minutes after injection of ligand. Data analysis was carried out as described previously[15].

## SUPPLEMENTARY NOTE 7

### Transformation function for mapping the acceptor track position to the donor channel

A transformation function mapping particle positions in the acceptor channel to the donor channel was measured as previously described[16]. Briefly, a grid of control points (grid spacing 1.5μm) in the acceptor and donor channel was measured by stepwise translating a diffraction limited fluorescent bead

(TetraSpeck, Thermo Fisher Scientific) across the microscope's aperture limited field of view using a two-axis piezo stage (Nano-BioS200 System, Mad City Labs). At each position, the bead was excited at 532 nm and 640 nm and imaged simultaneously using the dual-band TIRF - FRET filter configuration (**Methods)**. To measure a large set of control points, an automated routine in Metamorph (Molecular Devices) was used to translate the bead to a new grid position, image simultaneously the bead fluorescence in the donor and acceptor channel, and add the new image slice to an image stack file. A grid defined by 26 rows and 24 columns was recorded in the donor and acceptor channel resulting in an image stack of 624 images each showing a pair of control points.

To determine the mapping function from the recorded image stack, spatial positions of corresponding control points in the donor and acceptor channel were measured using the particle localization routine of the software Trackmate in ImageJ[17,18]. The positions of these control point pairs were then used to determine the local weighted mean transformation *tform_lwm*, which maps any position in the acceptor channel to the donor channel. To infer the transformation *tform_lwm* from the pairs of control points, we used the functions *fitgeotrans* with the transformation type *local weighted mean* and *transformPointsInverse* (Matlab Image Processing Toolbox, Mathworks)[19]. Individual single-molecule positions in the acceptor channel were then mapped to the donor channel by applying the inverse geometric transformation *transformPointsInverse* to the acceptor data. The calculated Target Registration Error (TRE) was on the order of 9 nm[20]. However due to limited particle localization accuracy the estimated mean registration error is on the order of ~25 nm.

## SUPPLEMENTARY NOTE 8

### Correction factors for calculating FRET efficiency

The $\alpha$ and $\gamma$ correction factors were measured manually using anticorrelated donor-acceptor fluorescence traces, with acceptor photobleaching preceding donor photobleaching. The $\alpha$ factor was calculated from

the elevated acceptor channel baseline after acceptor photobleaching. The γ factor was calculated from the ratio of intensity changes of donor and acceptor fluorophores before and after photobleaching[21]. Both measurements were carried out for each individual trajectory, which resulted in normally distributed histograms for both α and γ correction factors. The mean values of the observed distributions were determined by fitting to a single Gaussian function (**Supplementary Table 7** and **Supplementary Fig. 2**), which were then used as global correction factors in the workflow to determine FRET efficiencies. These values generally agreed with theoretical values estimated from the transmission spectra of elements in the optical path and the emission spectra of the fluorophores (**Extended Data Fig. 1e,f and Supplementary Fig. 1**; **Supplementary Table 1**). The δ factor was estimated from absorbance spectra of the two fluorophores to be 5.6% (**Supplementary Fig. 2**).

FRET was set to zero after donor tracking ended and to Not-a-Number (NaN) in the event of gap-closing[5]. To minimize the contribution of aberrant FRET efficiency values associated with donor fluorophore transitions to non-fluorescent or partially quenched states, the total intensity ($I_{Acc}$+$I_{Don}$) of individual trajectories was idealized using a three-state model using a segmental k-means (SKM) algorithm [22]. The model states include a dark state (total intensity is close to zero), a low intensity state (the intensity is partly attenuated by dye blinking or by temporary fluctuations due to particle movement) and a high fluorescence state. Anytime the total intensity is idealized to the dark or low state, the FRET efficiency is set to zero.[23]

## REFERENCES


1. Toomre, D. & Bewersdorf, J. A new wave of cellular imaging. *Annu Rev Cell Dev Biol* **26**, 285-314 (2010).
2. Brunstein, M., Teremetz, M., Herault, K., Tourain, C. & Oheim, M. Eliminating unwanted far-field excitation in objective-type TIRF. Part I. identifying sources of nonevanescent excitation light. *Biophys J* **106**, 1020-32 (2014).
3. Lanni, F., Waggoner, A.S. & Taylor, D.L. Structural organization of interphase 3T3 fibroblasts studied by total internal reflection fluorescence microscopy. *J Cell Biol* **100**, 1091-102 (1985).

4. Simon, S.M. Partial internal reflections on total internal reflection fluorescent microscopy. *Trends Cell Biol* **19**, 661-8 (2009).
5. Jaqaman, K. et al. Robust single-particle tracking in live-cell time-lapse sequences. *Nat Methods* **5**, 695-702 (2008).
6. Zheng, Q. et al. Electronic tuning of self-healing fluorophores for live-cell and single-molecule imaging. *Chem Sci* **8**, 755-762 (2017).
7. Pati, A.K. et al. Tuning the Baird aromatic triplet-state energy of cyclooctatetraene to maximize the self-healing mechanism in organic fluorophores. *Proc Natl Acad Sci U S A* **117**, 24305-24315 (2020).
8. Ishitsuka, Y. et al. Evaluation of Genetically Encoded Chemical Tags as Orthogonal Fluorophore Labeling Tools for Single-Molecule FRET Applications. *J Phys Chem B* **119**, 6611-9 (2015).
9. Vafabakhsh, R., Levitz, J. & Isacoff, E.Y. Conformational dynamics of a class C G-protein-coupled receptor. *Nature* **524**, 497-501 (2015).
10. Keppler, A. et al. A general method for the covalent labeling of fusion proteins with small molecules in vivo. *Nat Biotechnol* **21**, 86-9 (2003).
11. Sun, X. et al. Development of SNAP-tag fluorogenic probes for wash-free fluorescence imaging. *Chembiochem* **12**, 2217-26 (2011).
12. Brun, M.A., Tan, K.T., Nakata, E., Hinner, M.J. & Johnsson, K. Semisynthetic fluorescent sensor proteins based on self-labeling protein tags. *J Am Chem Soc* **131**, 5873-84 (2009).
13. Altman, R.B. et al. Cyanine fluorophore derivatives with enhanced photostability. *Nat Methods* **9**, 68-71 (2011).
14. Jiang, L.I. et al. Use of a cAMP BRET sensor to characterize a novel regulation of cAMP by the sphingosine 1-phosphate/G13 pathway. *J Biol Chem* **282**, 10576-84 (2007).
15. Donthamsetti, P. et al. Arrestin recruitment to dopamine D2 receptor mediates locomotion but not incentive motivation. *Mol Psychiatry* (2018).
16. Churchman, L.S., Okten, Z., Rock, R.S., Dawson, J.F. & Spudich, J.A. Single molecule high-resolution colocalization of Cy3 and Cy5 attached to macromolecules measures intramolecular distances through time. *Proc Natl Acad Sci U S A* **102**, 1419-23 (2005).
17. Tinevez, J.Y. et al. TrackMate: An open and extensible platform for single-particle tracking. *Methods* **115**, 80-90 (2017).
18. Schneider, C.A., Rasband, W.S. & Eliceiri, K.W. NIH Image to ImageJ: 25 years of image analysis. *Nat Methods* **9**, 671-5 (2012).
19. Goshtasby, A. Image registration by local approximation methods. *Image Vision Comput.* **6**, 255-261 (1988).
20. Sonka, M. & Fitzpatrick, J.M. Handbook of medical imaging. (SPIE, Bellingham, Wash. (1000 20th St. Bellingham WA 98225-6705 USA) :, 2000).
21. McCann, J.J., Choi, U.B., Zheng, L., Weninger, K. & Bowen, M.E. Optimizing methods to recover absolute FRET efficiency from immobilized single molecules. *Biophys J* **99**, 961-70 (2010).
22. Qin, F. Restoration of single-channel currents using the segmental k-means method based on hidden Markov modeling. *Biophys J* **86**, 1488-501 (2004).
23. Juette, M.F. et al. Single-molecule imaging of non-equilibrium molecular ensembles on the millisecond timescale. *Nat Methods* **13**, 341-4 (2016).